Supporting Information for

Operando video microscopy of Li plating and re-intercalation on graphite anodes during fast charging

Yuxin Chen[1], Kuan-Hung Chen[2], Adrian J. Sanchez[1], Eric Kazyak[1], Vishwas Goel[2], Yelena Gorlin[3], Jake Christensen[3], Katsuyo Thorton[2], Neil P. Dasgupta[1,2*]

[1] Department of Mechanical Engineering, University of Michigan, Ann Arbor, MI 48109, USA

[2] Department of Materials Science & Engineering, University of Michigan, Ann Arbor, MI 48109, USA

[3] Robert Bosch LLC, Research and Technology Center, Sunnyvale, CA 94085, USA

*Corresponding Author: ndasgupt@umich.edu

Supplementary figures

Figure S1 – XRD spectrum and corresponding optical microscope images of graphite, LiC_{12} and LiC_6.

Figure S2 – 900um x 740um field of view images for the still frames during C/10 charging. The same frames with smaller field of view are shown in **Fig. 2**.

Figure S3 – Still frames of 6C charging with 85mAh/g cutoff. The same frames with smaller field of view are shown in **Fig. 3**.

Figure S4 – XRD spectrum and calculated graphite SoC after fast charging

Figure S5 – SEM images of plated Li showing that the color change during dead Li formation is caused by increase in the surface roughness of plated Li.

Figure S6 – OCV rest and C/5 discharge after lithium plating caused by overcharging.

Figure S7 – Still frames of OCV rest and C/5 discharge after the 6C charging shown in **Fig. 3 and S2**. The same frames with smaller field of view are shown in **Fig. 4**.

Figure S8 – Still frames of OCV rest and C/5 discharge after the 6C charging with 121mAh/g cutoff (cell B). The voltage profile and zoom-in images of this cell are shown in **Fig. 6**.

Figure S9 – Still frames of the OCV rest after C/10 charging. No Li plating was observed during charging, and during the OCV rest, no deflection was observed in the voltage profile, and no peak was observed in the dV/dt profile.

Figure S10 – Cross sectional images of a coin cell electrode 20min after disassembly and 110min after disassembly.

Figure S11 – Still frames of C/5 discharge immediately following a 6C charging with 85mAh/g cutoff. The voltage profile and zoom-in images of this cell are shown in **Fig. 8**.

Figure S12 – Voltage traces and dV/dt curves of a pouch cell after C/2 charging.

Figure S13 – Post-mortem optical images of the three pouch cells in **Fig. 9**. Severe Li plating was observed on the graphite electrodes.

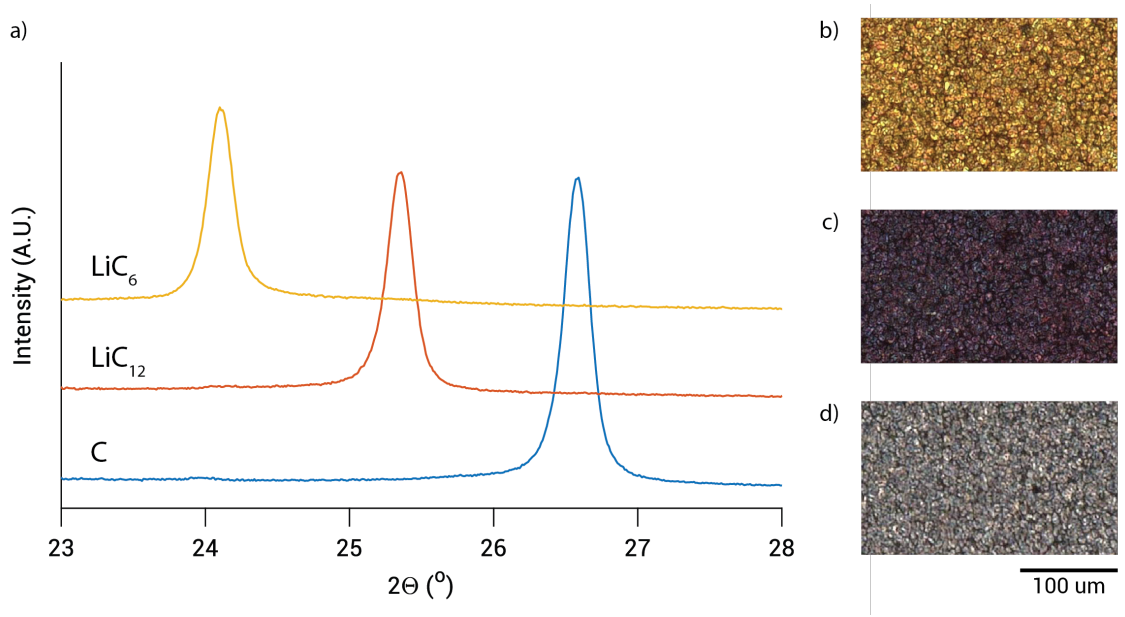

Figure S1 a) XRD spectra of graphite, LiC_{12} and LiC_6 and **b – d)** corresponding optical images.

Two coin cells were lithiated to LiC_{12} and LiC_6 at C/10 charging rate. The graphite electrodes were retrieved and rinsed with DMC. XRD and optical microscopy were performed on both lithiated electrodes as well as an unlithiated electrode.

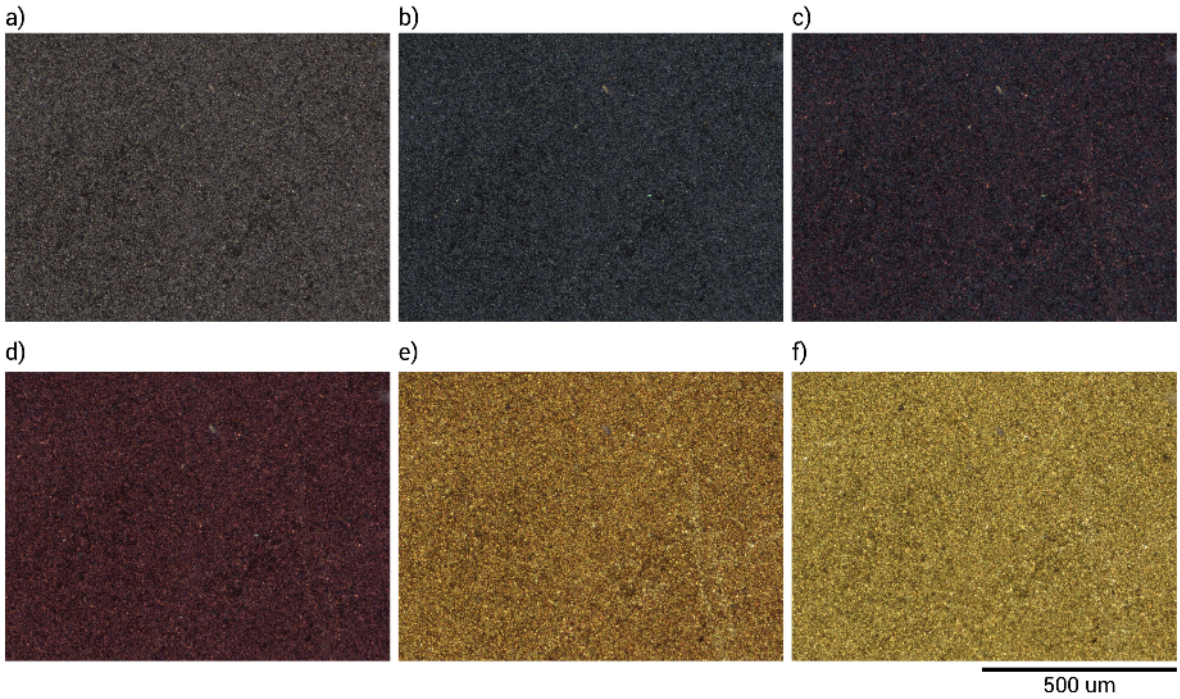

Figure S2 900um x 740um field-of-view images for the still frames during C/10 charging. The same frames with smaller field of view are shown in Fig. 2.

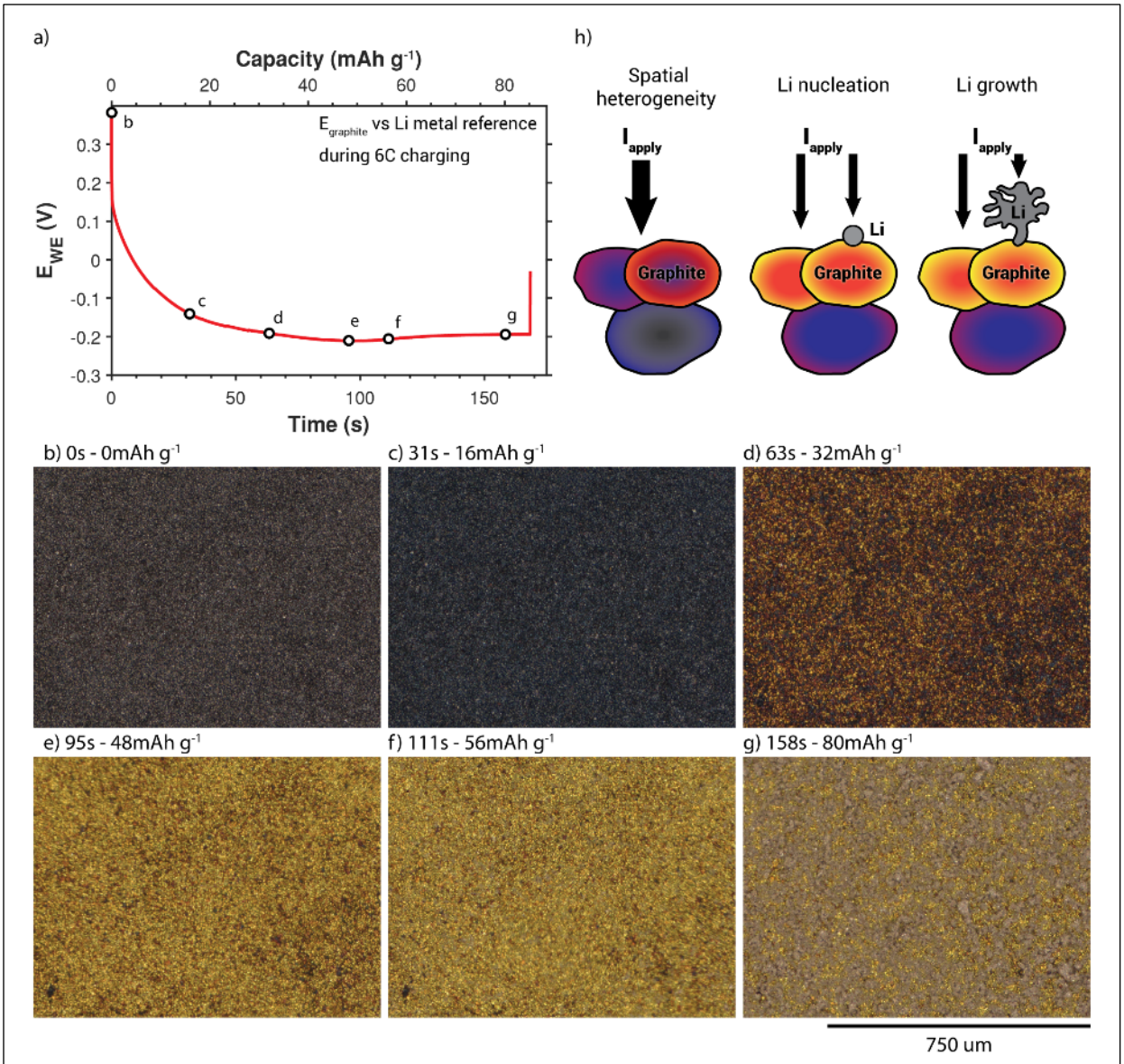

Figure S3 Still frames of 6C charging with 85mAh/g cutoff. The same frames with smaller field of view are shown in Fig. 3.

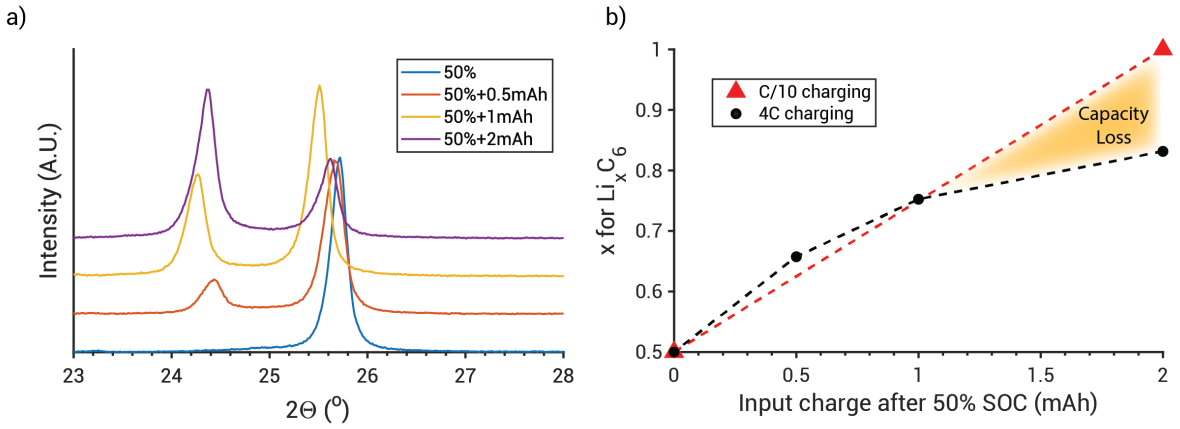

Figure S4 a) XRD spectra of graphite anodes extracted from four coin cells after various amounts of charge passed at 4C; **b)** Calculated average Li content based on the XRD patterns after 4C charging and C/10 charging of coin cells.

Four coin cells were slow charged to 50% SoC at C/10, and then 0 mAh, 0.5 mAh, 1 mAh and 2 mAh of charge was passed at a 4C rate, respectively. The cells were rested at OCV for >30min before the graphite electrodes were extracted and rinsed with DMC. XRD analysis was then performed. The average Li content in the graphite was calculated based on the intensity of the LiC_6 and LiC_{12} peaks [1]. After 2 mAh of charge was passed, the electrode that was charged at 4C had a lower average Li content than the electrode that was charged at C/10. This confirms that the reaction pathway transitioned away from Li intercalation during fast charging as a result of Li plating.

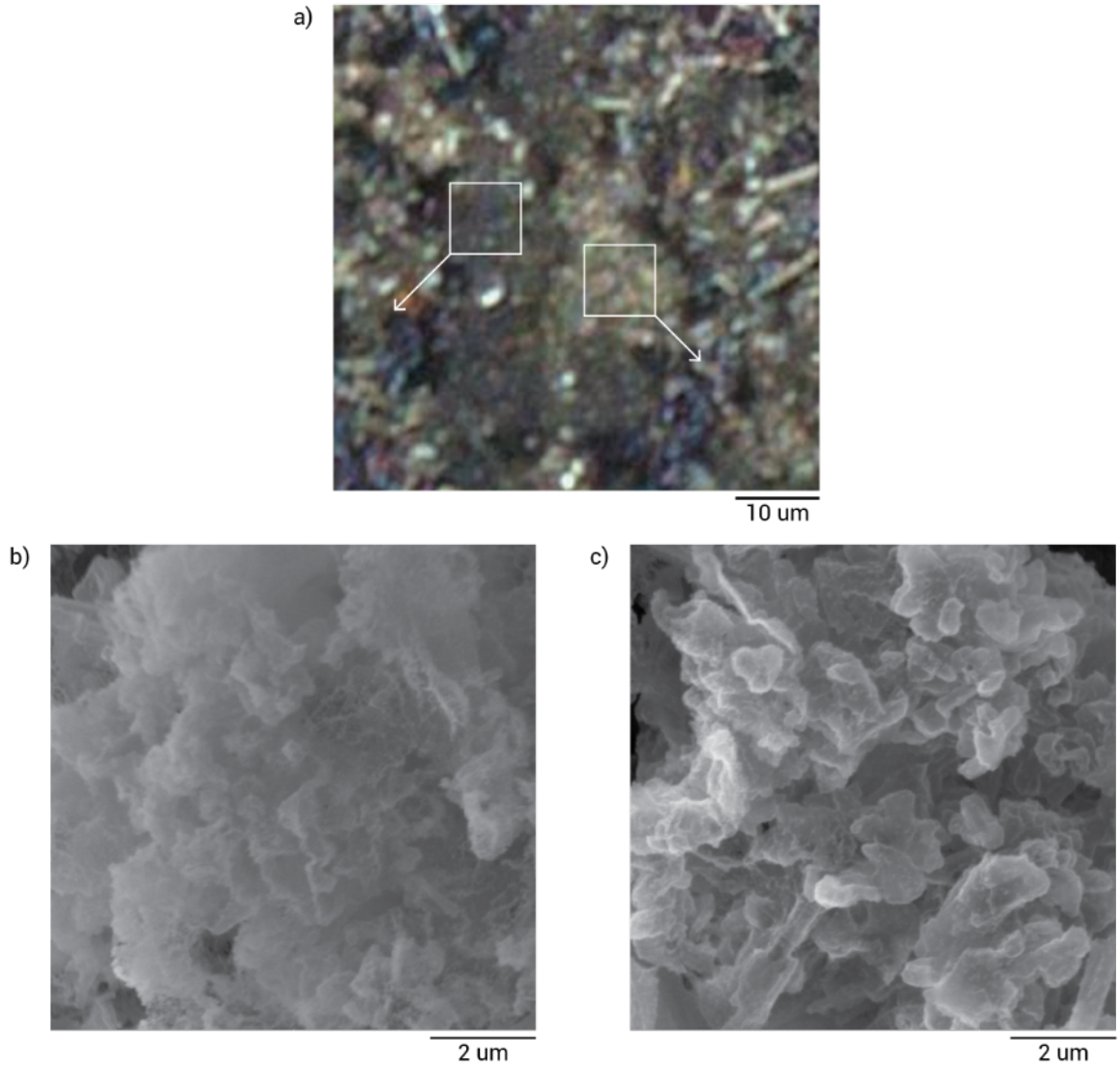

Figure S5 Optical and SEM images of dead Li on graphite. The visualization cell underwent 6C charging until 100 mAh g^{-1}, starting from 0.4 V vs Li/Li^{+}. It was then rested at OCV for 10 min to allow dead Li formation. The graphite WE was then harvested and rinsed with anhydrous dimethyl carbonate solvent to remove excess electrolyte. The sample was prepared and transferred into SEM without air exposure. A dead Li structure was imaged with **a)** optical microscopy and **b-c)** SEM.

The optically black portion of the dead Li structure (**Fig. S3 b**) results from the collapse of the SEI layer on the plated Li metal surface during re-intercalation. This roughening reduces the optical reflectance of the surface, causing this local region to appear black under optical microscope. In contrast, the portion of plated region that retains a gray luster (**Fig. S3 c**) exhibits less surface roughness.

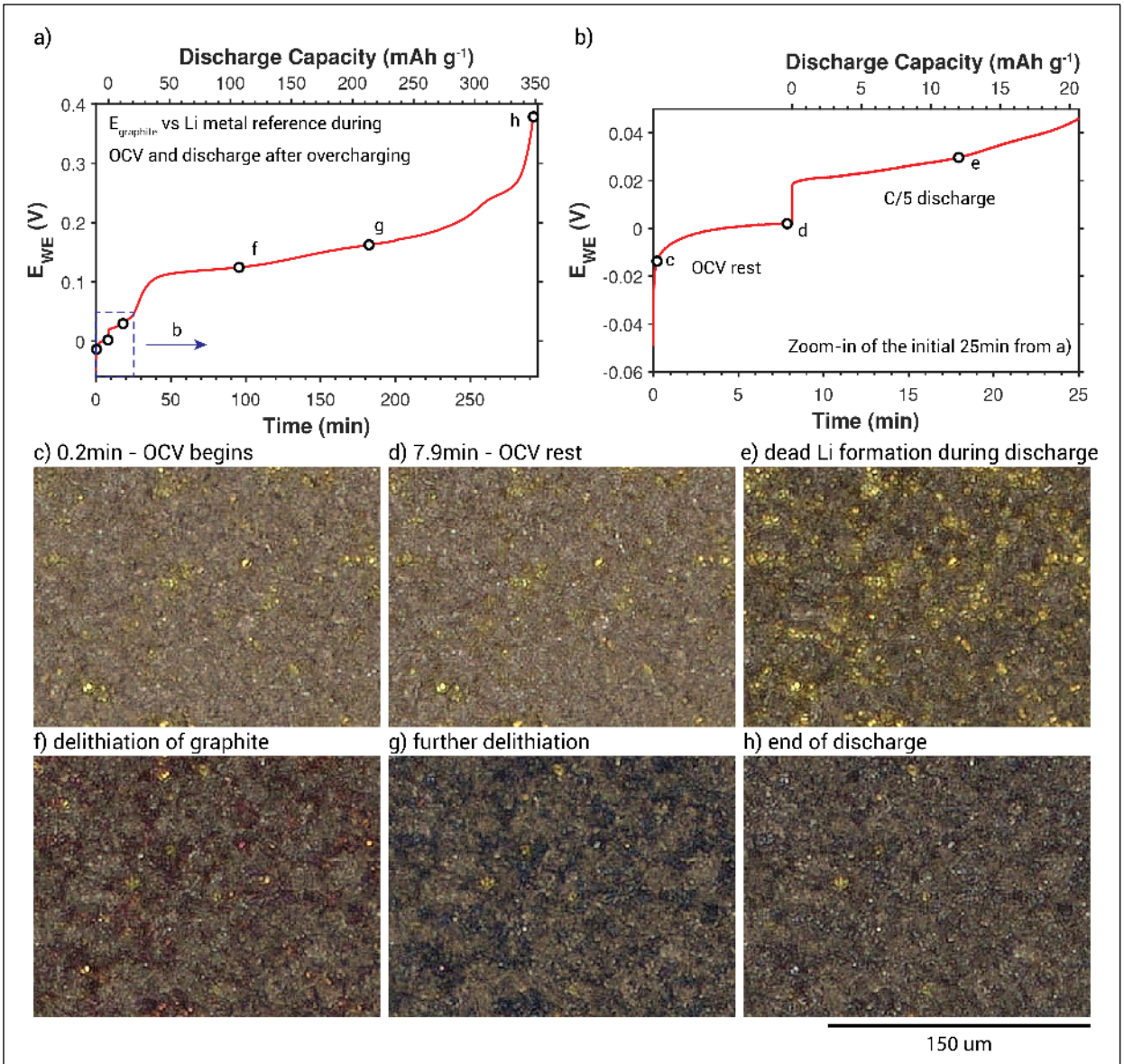

Figure S6 OCV rest and C/5 discharge after 6C overcharging of 26.6mAh g^{-1}. This electrode was fully lithiated to 20mV vs Li/Li^+ at C/10 (349mAh g^{-1}) before being charged at 6C for an overcharge of 26.6mAh g^{-1}. During the OCV rest, no obvious change was observed for both the graphite and the plated Li.

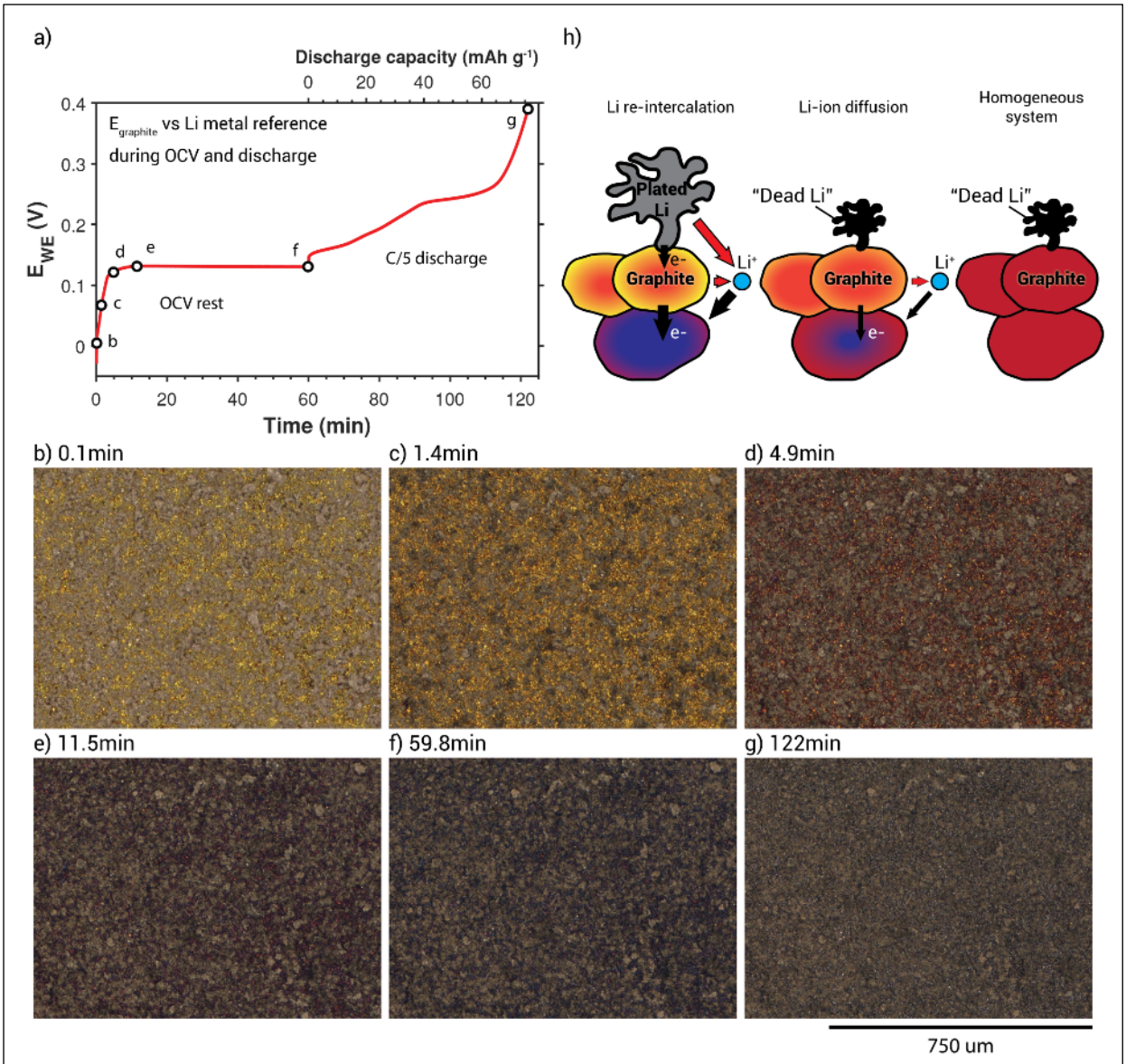

Figure S7 Still frames of OCV rest and C/5 discharge after the 6C charging shown in Fig. 3 and S2. The same frames with smaller field of view are shown in Fig. 4.

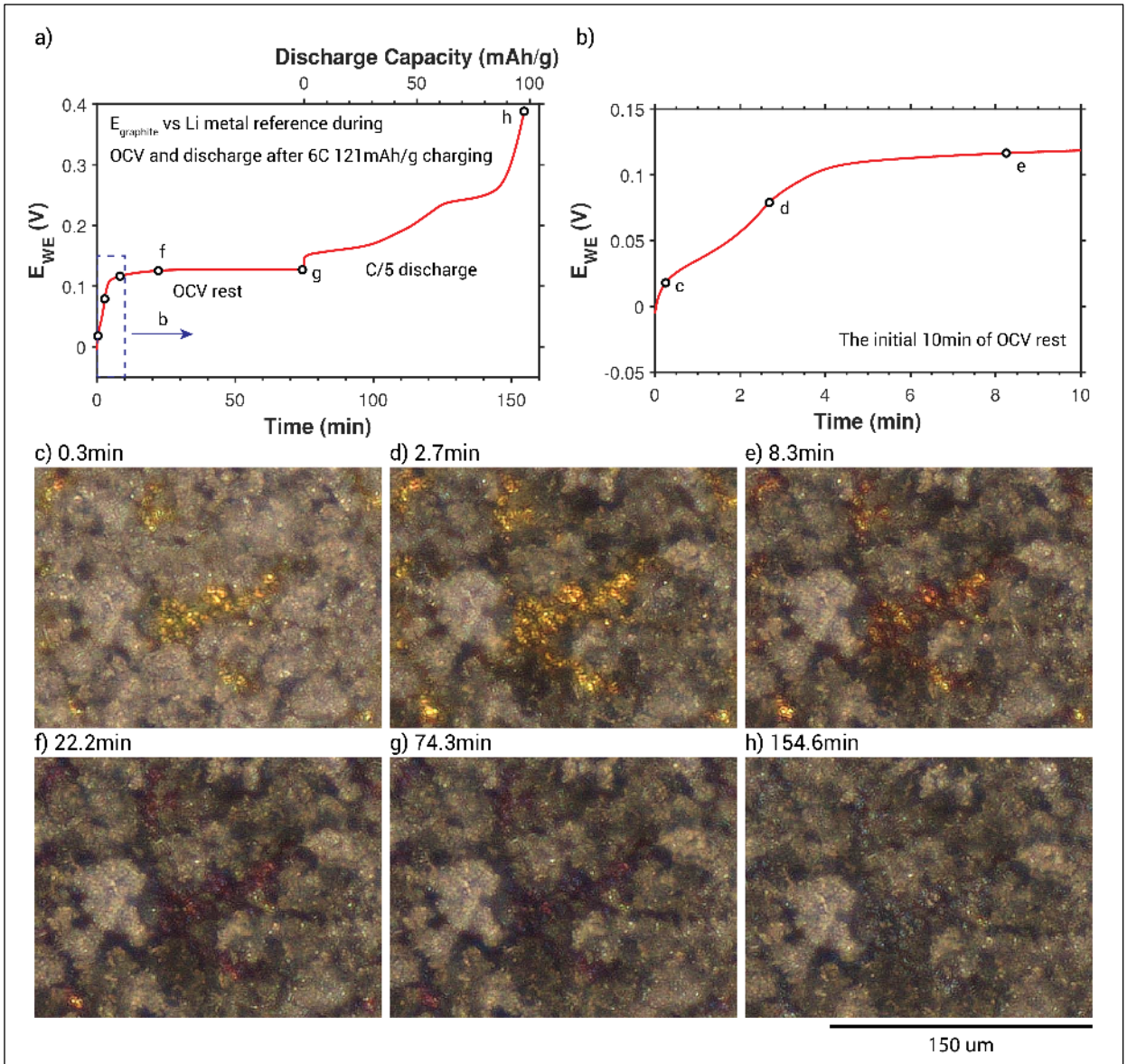

Figure S8 Still frames of OCV rest and C/5 discharge after the 6C charging with 121mAh/g cutoff. The voltage profile and zoomed-in images of this cell are shown in **Fig. 6**.

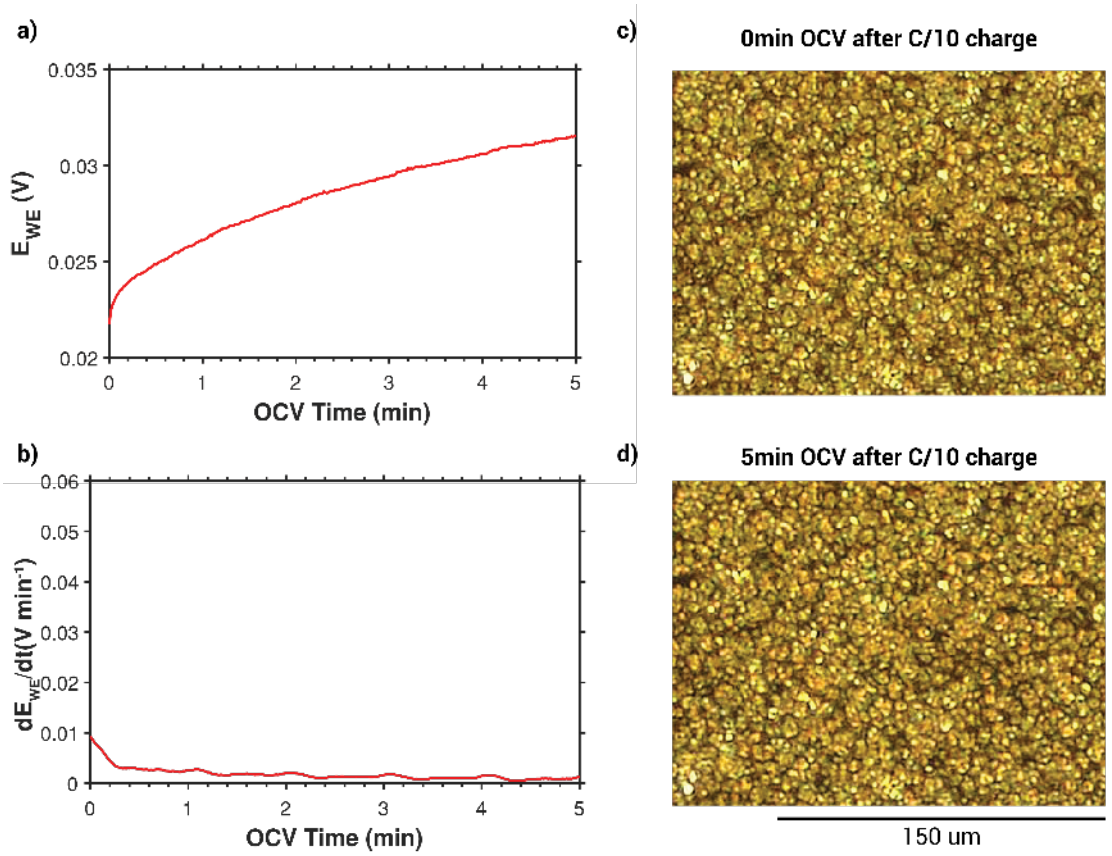

Figure S9 Still frames of the OCV rest after C/10 charging. No Li plating was observed during charging, and during the OCV rest, no deflection was observed in the voltage profile and no peak was observed in the dV/dt profile.

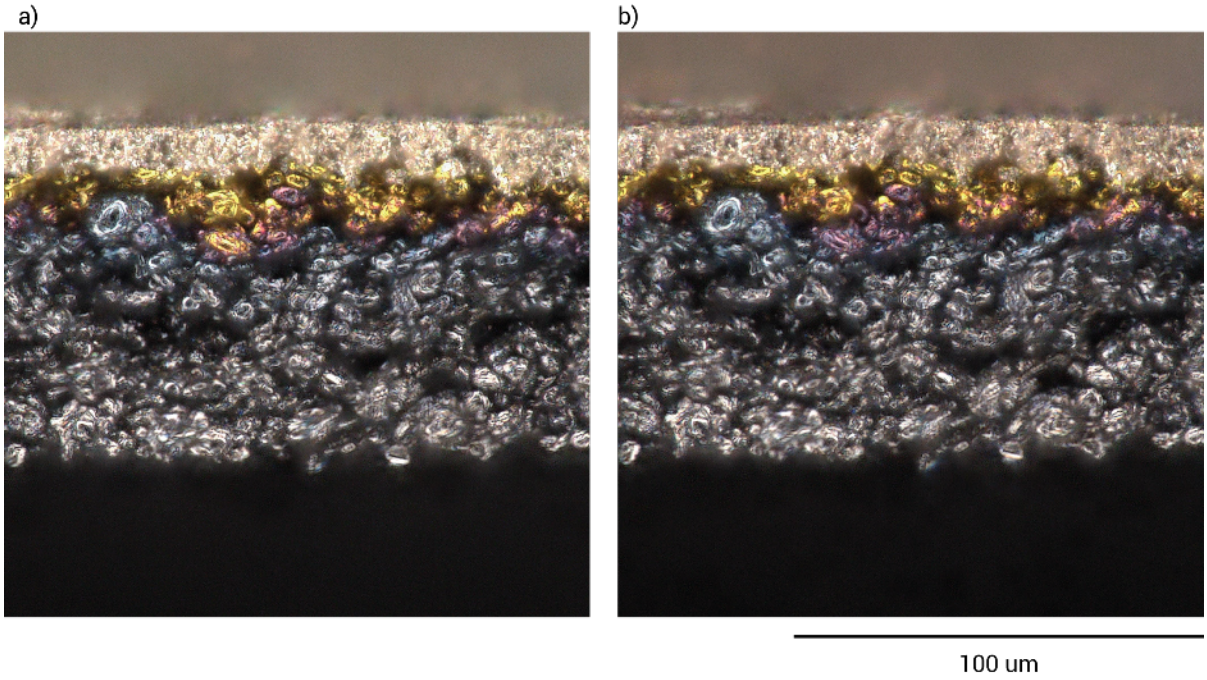

Figure S10 A coin cell was fast charged and then immediately disassembled and rinsed. Cross-sectional images were taken **a)** 15min after disassembling and **b)** 110min after disassembling. The sample was stored in Ar without any air exposure in the time between the images were taken.

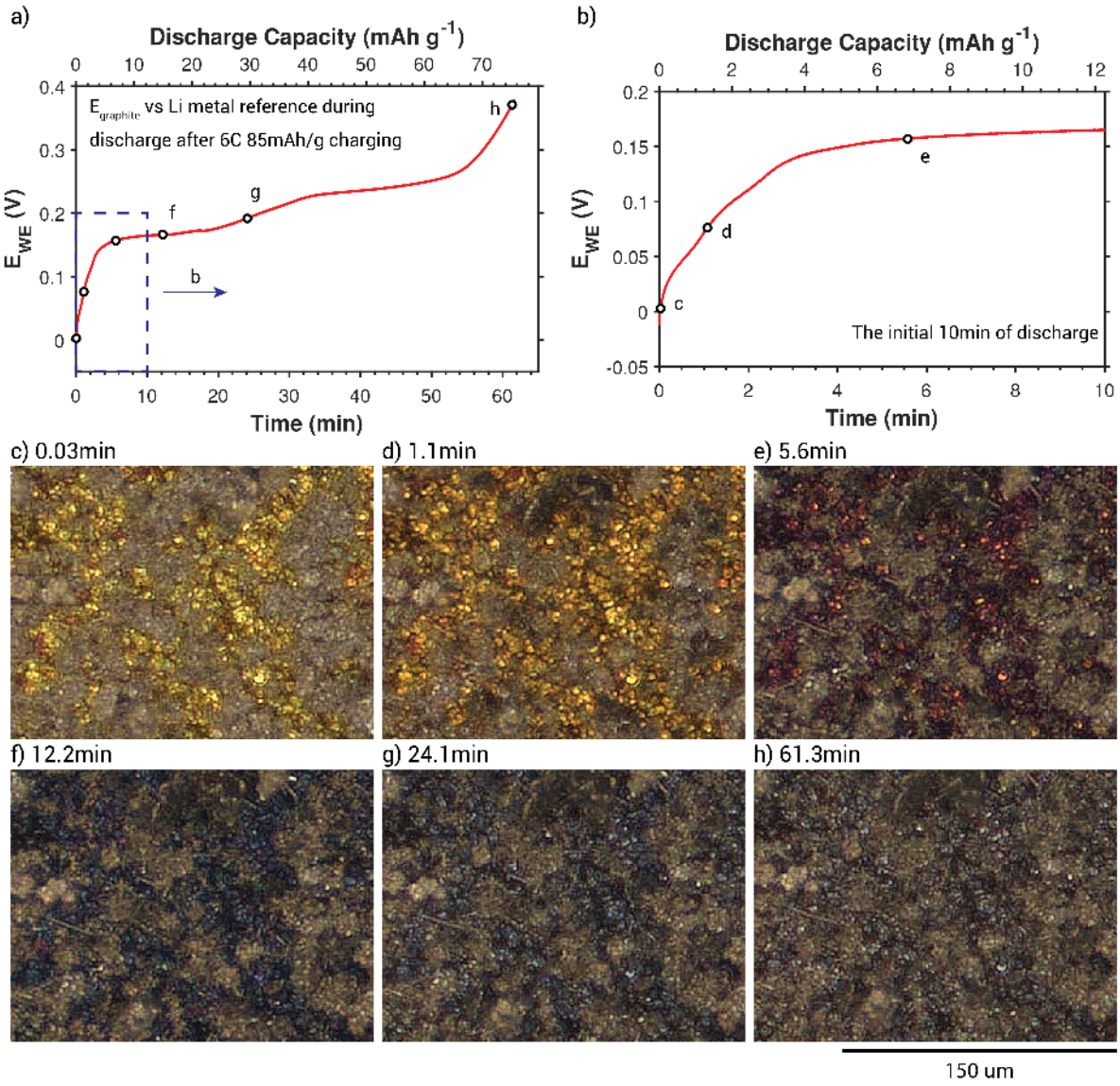

Figure S11 Still frames of C/5 discharge immediately following a 6C charging with 85mAh/g cutoff. The voltage profile and zoom-in images of this cell are shown in **Fig. 8.**

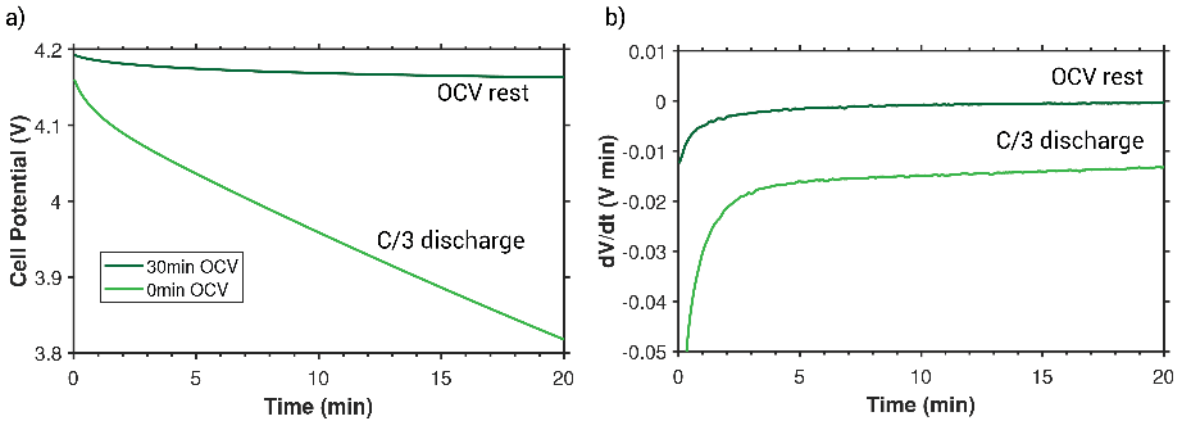

Figure S12 a) Voltage traces and **b)** dV/dt curves of a pouch cell after C/2 charging. The graphite-NMC pouch cell was charged using a constant current-constant voltage (CC-CV) protocol at a C/2 rate until 4.2V and then held at the constant voltage until the current decreased to C/10. It was then rested at OCV for 0 min (1st cycle) and 30 min (2nd cycle). After that it was discharged at a C/2 rate until 3V. No Li re-intercalation plateau was observed during the OCV or discharge step. No peak was observed in the dV/dt curves.

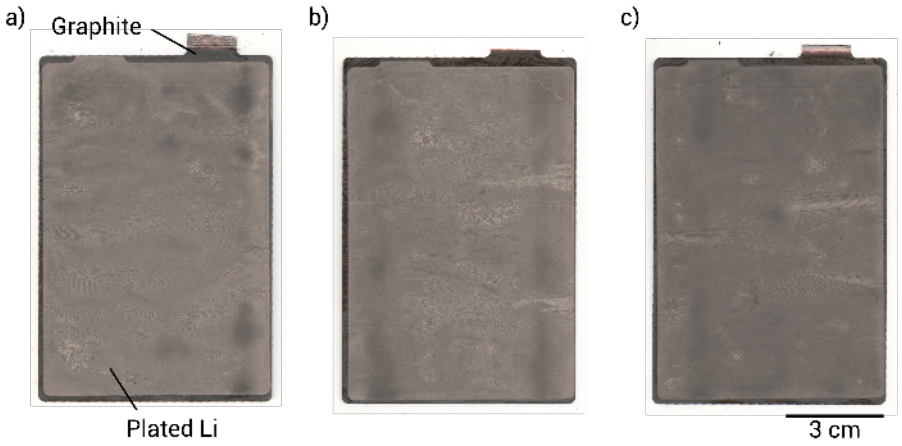

Figure S13 Post-mortem optical images of the three cells in **Fig. 9** after five 6C cycles. Li plating was observed on the three cells with **a)** 0min, **b)** 5min, and **c)** 30min OCV rest between charge and discharge half cycles.

Table S1. Discharge capacity and Coulombic efficiency of the three pouch cells with 0 min, 5 min and 30 min OCV rest between 6C charge and C/2 discharges

OCV rest time	Discharge capacity	Coulombic efficiency
0 min	0.137 Ah	96.5%
5 min	0.135 Ah	95.7%
30 min	0.138 Ah	97.2%

Model setup

To simulate the distribution of the current density at the WE/electrolyte interface, a 2D axisymmetric model was setup in COMSOL Multiphysics®. Figure S11 shows the labeled schematic of the visualization cell used for the study, along with the physical processes being considered. The dotted line represents the symmetry axis for the computational domain. The model equations and associated parameters can be found in our previous work [2], except that the electrochemical reaction at the Li/electrolyte interface where the reaction flux, J, at the Li/electrolyte interface was calculated by using Eq. S1 [3]. Using this model, we solve for the diffusion and migration of Li-ions along with electrochemical reaction, electronic conduction, solid-state diffusion in the porous electrode and electrochemical reaction at the Li/electrolyte interface. The Li metal, or CE, is grounded while a constant current density boundary condition is applied at the WE/current collector interface.

$$J = k \times \left(c_{Li} \exp\left(\frac{0.5F}{RT}\eta\right) - c_e \exp\left(\frac{-0.5F}{RT}\eta\right)\right) \quad \text{(S1)}$$

where k is the reaction rate constant, c_{Li} is concentration of metallic Lithium, which is equal to the inverse of the molar volume of Li, c_e is the electrolyte concentration, and η is the overpotential as defined in [2]. The values of parameters in Eq. 1 were obtained from [3] and set as $k = 3.5 \times 10^{-8}\, m/s$ and $c_{Li} = 7.69 \times 10^{4}\, mol/m^3$.

A custom triangular mesh was used to discretize the computational domain. Mesh refinement was used near the corners and within WE; the maximum element size within WE was kept to be $1\ \mu m$ to ensure sufficient refinement level. The model equations were solved using the multifrontal massively parallel sparse direct solver (MUMPS) [4] and a backward differential formula (BDF) scheme for time-stepping with a relative tolerance of 1×10^{-6}.

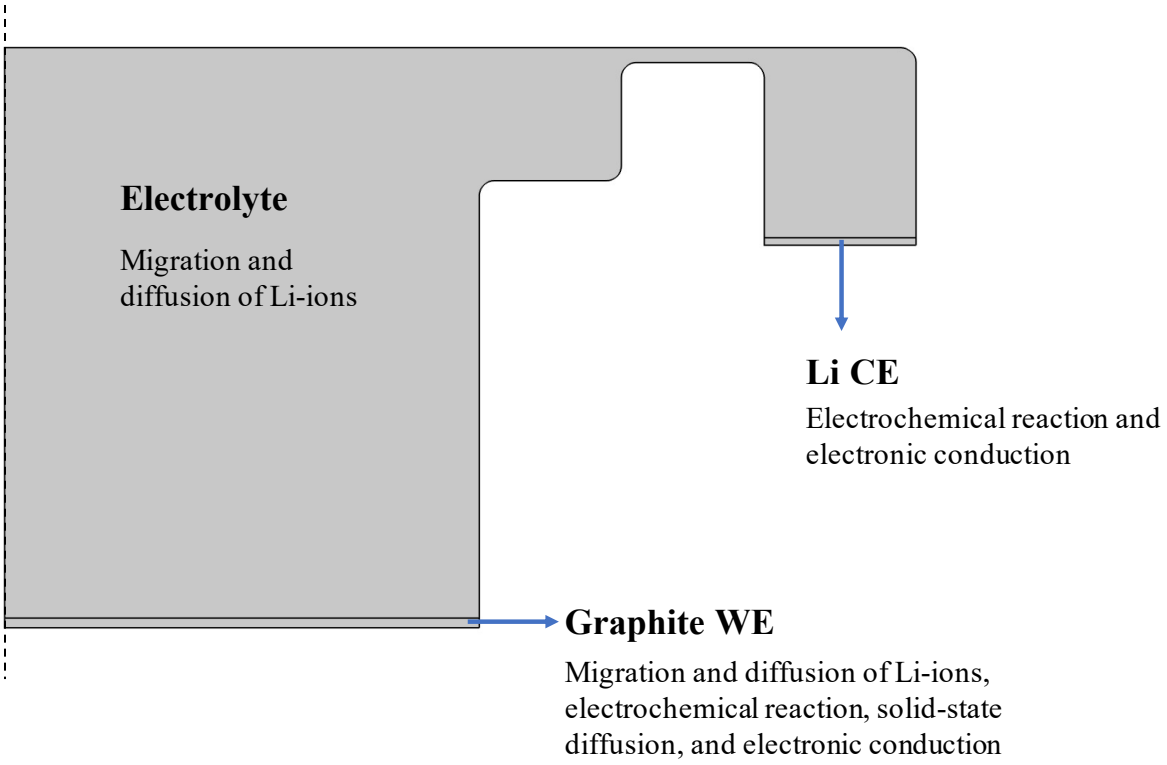

Figure S14 Schematic of the visualization cell used in this study. The dashed line represents the symmetry axis for the model.

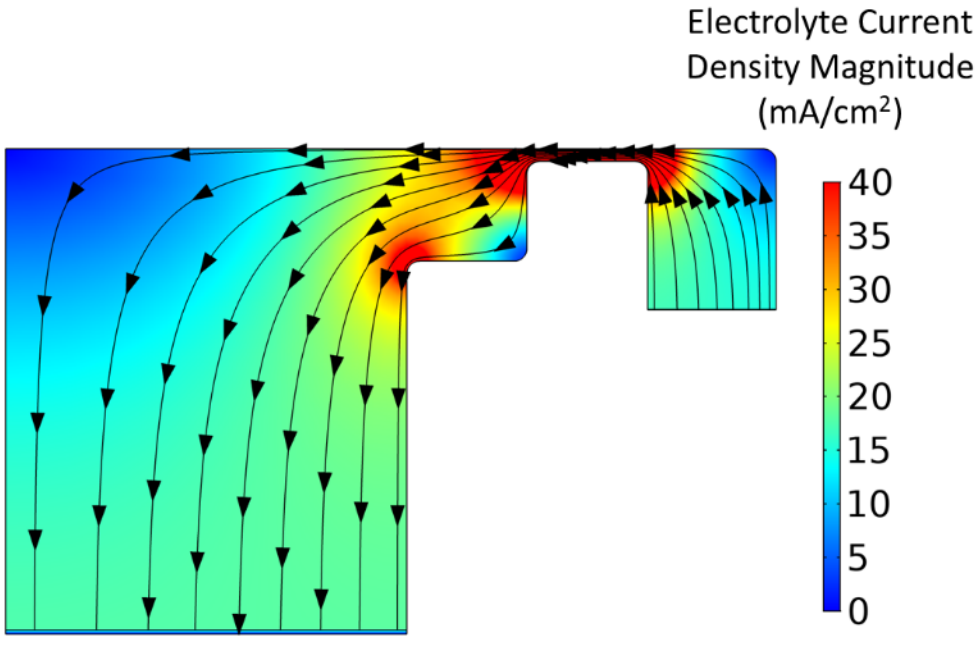

Figure S15 Simulated electrolyte current density during 6C charging.

References

[1] K. P. C. Yao, J. S. Okasinski, K. Kalaga, I. A. Shkrob, and D. P. Abraham, "Quantifying lithium concentration gradients in the graphite electrode of Li-ion cells using: Operando energy dispersive X-ray diffraction," *Energy Environ. Sci.*, vol. 12, no. 2, pp. 656–665, Feb. 2019.

[2] K. H. Chen *et al.*, "Efficient fast-charging of lithium-ion batteries enabled by laser-patterned three-dimensional graphite anode architectures," *J. Power Sources*, vol. 471, p. 228475, Sep. 2020.

[3] K. N. Wood *et al.*, "Dendrites and pits: Untangling the complex behavior of lithium metal anodes through operando video microscopy," *ACS Cent. Sci.*, vol. 2, no. 11, pp. 790–801, 2016.

[4] P. R. Amestoy, I. S. Duff, and J. Y. L'Excellent, "Multifrontal parallel distributed symmetric and unsymmetric solvers," *Comput. Methods Appl. Mech. Eng.*, vol. 184, no. 2–4, pp. 501–520, 2000.